

## BASIC SCIENCES

# Single-Cell RNA Sequencing and Assay for Transposase-Accessible Chromatin Using Sequencing Reveals Cellular and Molecular Dynamics of Aortic Aging in Mice

Wenhui Xie,\* Yilang Ke,\* Qinyi You,\* Jing Li, Lu Chen, Dang Li, Jun Fang, Xiaofeng Chen, Yuanyuan Zhou, Liangwan Chen, Huashan Hong<sup>ID</sup>

**OBJECTIVE:** The impact of vascular aging on cardiovascular diseases has been extensively studied; however, little is known regarding the cellular and molecular mechanisms underlying age-related vascular aging in aortic cellular subpopulations.

**APPROACH AND RESULTS:** Transcriptomes and transposase-accessible chromatin profiles from the aortas of 4-, 26-, and 86-week-old C57/BL6J mice were analyzed using single-cell RNA sequencing and assay for transposase-accessible chromatin sequencing. By integrating the heterogeneous transcriptome and chromatin accessibility data, we identified cell-specific TF (transcription factor) regulatory networks and open chromatin states. We also determined that aortic aging affects cell interactions, inflammation, cell type composition, dysregulation of transcriptional control, and chromatin accessibility. Endothelial cells 1 have higher gene set activity related to cellular senescence and aging than do endothelial cells 2. Moreover, construction of senescence trajectories shows that endothelial cell 1 and fibroblast senescence is associated with distinct TF open chromatin states and an mRNA expression model.

**CONCLUSIONS:** Our data provide a system-wide model for transcriptional and epigenetic regulation during aortic aging at single-cell resolution.

**GRAPHIC ABSTRACT:** A graphic abstract is available for this article.

**Key Words:** aorta ■ endothelial cells ■ fibroblasts ■ inflammation ■ transcriptome

**A**ging is a major risk factor for cardiovascular disorders, with over 50% of clinical cardiovascular disorders occurring in the elderly.<sup>1</sup> The age-related structural and functional degenerative changes in arteries support the development of vascular diseases.<sup>2</sup> In turn, vascular diseases accelerate the process of vascular aging (VA), thus forming a vicious circle.<sup>3</sup> Although we have previously attempted to treat aortopathy,<sup>4,5</sup> further investigations into effective treatment strategies are warranted. Characteristics of VAs include endothelial dysfunction, vascular remodeling, inflammation, calcification, and stiffness. However, the molecular and cellular processes

underlying the age-related progressive changes of vascular function and structure remain to be elucidated.

**See accompanying editorial on page 172**  
**See cover image**

Recent advances in droplet-based technologies have greatly enhanced single-cell sequencing throughput, facilitating a better understanding of aortic heterogeneity.<sup>6,7</sup> Although powerful for identifying cell type heterogeneity in complicated tissues, single-cell RNA sequencing fails to detect the landscape of chromatin accessibility. The changes

Correspondence to: Huashan Hong, MD, PhD, Department of Geriatrics, Fujian Key Laboratory of Vascular Aging, Fujian Institute of Geriatrics, Fujian Medical University Union Hospital, Fujian Medical University, Fuzhou, Fujian, China, Email 15956159898@163.com; or Liangwan Chen, MD, PhD, Department of Cardiac Surgery, Fujian Medical University Union Hospital, Fuzhou, Fujian, China, Email chenliangwan@tom.com

\*W. Xie, Y. Ke, and Q. You contributed equally.

Supplemental Material is available at <https://www.ahajournals.org/doi/suppl/10.1161/ATVBAHA.121.316883>.

For Sources of Funding and Disclosures, see page 170.

© 2021 American Heart Association, Inc.

*Arterioscler Thromb Vasc Biol* is available at [www.ahajournals.org/journal/atvb](http://www.ahajournals.org/journal/atvb)

## Nonstandard Abbreviations and Acronyms

<b>EC</b>	endothelial cell
<b>IAR</b>	increased accessibility region
<b>IL</b>	interleukin
<b>NF-κB</b>	nuclear factor kappa B
<b>scATAC-seq</b>	single-cell assay for transposase-accessible chromatin sequencing
<b>scRNA-seq</b>	single-cell RNA sequencing
<b>TF</b>	transcription factor
<b>TGF-β</b>	transforming growth factor beta
<b>TNF-α</b>	tumor necrosis factor alpha
<b>VA</b>	vascular aging
<b>VSMC</b>	vascular smooth muscle cell

in chromatin accessibility have been linked to cellular senescence<sup>8</sup>; however, the chromatin accessibility dynamics involved in aortic aging at the single-cell level is lacking. Therefore, transcriptomic profiling overlaying epigenetic information can provide a more complete picture of how these expression profiles are regulated during aortic aging.

Herein, we obtained single-cell transcriptional and chromatin accessibility data sets for mice aorta at 3 different ages (4, 26, and 86 weeks of age), representing different stages of aortic aging. From these data sets, we identified cell type-specific gene and chromatin accessibility markers, as well as gene regulatory networks unique to each cell type. Furthermore, we revealed that aortic aging affects cell communication, inflammation, cell type composition, dysregulation of transcriptional control, and chromatin accessibility. Thus, our study provides a comprehensive understanding of aortic aging at the transcriptional and epigenetic levels, thereby facilitating the development of new therapies for human age-related cardiovascular diseases.

## METHODS

### Data Availability

The data that support the findings of this study are available from the corresponding author upon reasonable request. All single-cell RNA sequencing (scRNA-seq) and single-cell assay for transposase-accessible chromatin sequencing (scATAC-seq) data are available from the Gene Expression Omnibus database under the accession number GSE164585.

### Animals

Sex differences in the rate of VA have been attributed to changes in sex hormones that occur with aging in females and males. Specifically, estrous cycles and menopause in female mice might cause data variability; thus, aortas were harvested from 4-, 26-, and 86-week-old male C57/BL6J mice (please see the Major Resources Table in the *Supplemental Material*), following 2 intracardiac perfusions with PBS (Hyclone, South

## Highlights

- Aortic single-cell transcriptional and epigenetic profiles showed 15 cell subpopulations with cell type-specific gene and chromatin accessibility markers, including endothelial cell 1, endothelial cell 2, and lymphatic endothelial cells.
- Aortic aging affects cell interactions, inflammation, cell type composition, dysregulation of transcriptional control, and chromatin accessibility.
- Senescence trajectory analysis revealed cell type-specific TFs (transcription factors) that regulate aortic aging.
- Characterizing transcriptional and epigenetic dynamics during aortic aging provides insights into the vascular health of patients with age-related vascular diseases.

Logan, UT). For each of the two major single-cell experiments, 2 biological replicates from each time point (2 mice per age group) were used. The isolated aorta included the ascending aorta, aortic arch, and thoracic aorta. Single cell and single nuclei from dissociated aortas were prepared for scRNA-seq and scATAC-seq library preparation and sequencing. All experimental procedures were approved by the Institutional Animal Care and Use Committee of Fujian Medical University (Fuzhou, Fujian, China) and performed according to the national Laboratory Animals Regulations and Fujian Regulations of Laboratory Animal Management. All animals were anesthetized with 1% pentobarbital sodium via intraperitoneal injection (30 mg/kg). Detailed Methods are provided in *Supplemental Methods*.

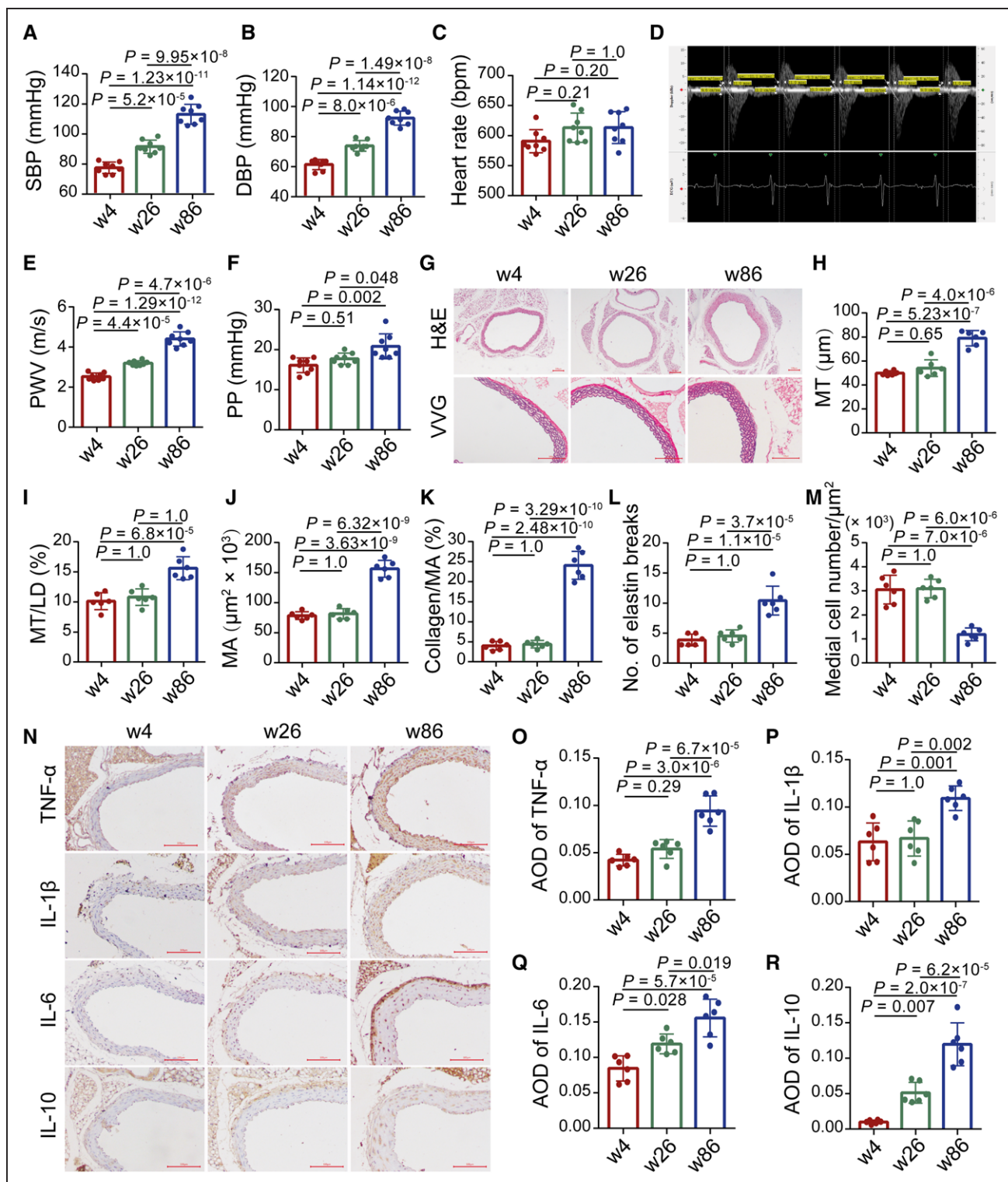
## Statistical Analysis

Data normal distribution and homogeneity of variance were evaluated using the Shapiro-Wilk normality method and Levene method, respectively. For normally distributed data with equal variance, *P* values were assessed between 2 groups using a 2-tailed Student *t* test and 1-way ANOVA followed by the Bonferroni post test for multiple comparisons. For data with non-normal distribution or uneven variance, the Mann-Whitney *U* test and Kruskal-Wallis test, followed by the Nemenyi post test, were used to compare 2 groups or multiple groups. *P*<0.05 was considered statistically significant. Data were analyzed using the R (version 3.6.2) software.

## RESULTS

### Changes in Physiological Function, Structure, and Inflammation During Aortic Aging

To assess the dynamic changes in aortic physiological parameters during aging, we examined wild-type male C57/BL6J mice divided into 3 age groups: mice at 4, 26, and 86 weeks. We observed that systolic and diastolic blood pressure increased with age, while the heart rate did not change (Figure 1A through 1C). Arterial stiffness is the hallmark of VAs. Thus, pulse wave velocity—a gold

**Figure 1. Evidence of aortic aging in mice.**

**A–C**, Systolic blood pressure (SBP), diastolic blood pressure (DBP), and heart rate in mice at different ages. n=8 mice. **D**, Pulse wave was measured using a noninvasive Doppler blood flow monitor in mice. **E**, Thoracoabdominal aorta value in mice. n=8 mice. **F**, Pulse pressure (PP; PP=SBP-DBP) in mice. n=8 mice. **G–M**, Vascular remodeling indicators, namely media thickness (MT), MT/lumen diameter (LD), media area (MA), collagen/MA, elastin breaks, and medial cell number, were analyzed using H&E (hematoxylin-eosin) and VVG (Verhoeff-van Gieson) staining in mouse thoracic aorta. n=6 mice. **N–R**, Expression levels of inflammatory cytokines, namely TNF-α (tumor necrosis factor alpha), IL (interleukin)-1β, IL-6, and IL-10, detected via immunohistochemistry. n=6 mice. Data are expressed as mean $\pm$ SD. P determined using 1-way ANOVA followed by the Bonferroni post test.

standard for detecting arterial stiffness—was used to assess aortic aging. Similar to the changes in blood pressure, pulse wave velocity value increased significantly with age (Figure 1D and 1E).

We also measured pulse pressure widening to assess arterial stiffness. Although we did not observe changes in pulse pressure between 4- and 26-week-old mice, a significant increase was noted in 86-week-old mice (Figure 1F). Morphologically, vascular remodeling related to aging, including increased media thickness, increased ratio of media thickness to lumen diameter, increased media area, increased ratio of collagen content to media area, elastin breaks, and decreased number of medial cells, was observed (Figure 1G through 1M).

Inflammation status was also observed via immunohistochemistry. Results showed that the expression of proinflammatory markers, namely TNF- $\alpha$  (tumor necrosis factor alpha), IL (interleukin)-1 $\beta$ , and IL-6, was significantly elevated in the thoracic aorta of 86-week-old mice compared with that in 4- and 26-week-old mice. Moreover, we observed increased expression of IL-10—an anti-inflammatory marker—in the thoracic aorta of 86-week-old mice (Figure 1N through 1R; Figure S1A).

## Single-Cell Profile of Aortic Aging

To further explore dynamic changes in molecular characteristics at the single-cell level during aortic aging, we performed 10x scRNA-seq on aortic tissues from 6 mice each at 4, 26, and 86 weeks of age (Figure 2A). Individual samples were independently assessed to select cells expressing >500 genes and genes expressed in >5 cells. Cells with >10% mitochondrial-derived genes were screened out and doublets were removed. All samples were then combined,<sup>9</sup> yielding 28014 cells (Table S1). We also regressed out heterogeneity associated with the cell cycle stage before performing cluster analysis to avoid within-cell type heterogeneity, which might blur clusters of cell types or cause cells in similar cell cycle stages to create new clusters.<sup>10</sup> After performing this correction, cells at different cell cycle stages were relatively evenly distributed, indicating that the correction was successful (Figure S1B). These 28014 cells were then used for subsequent analyses.

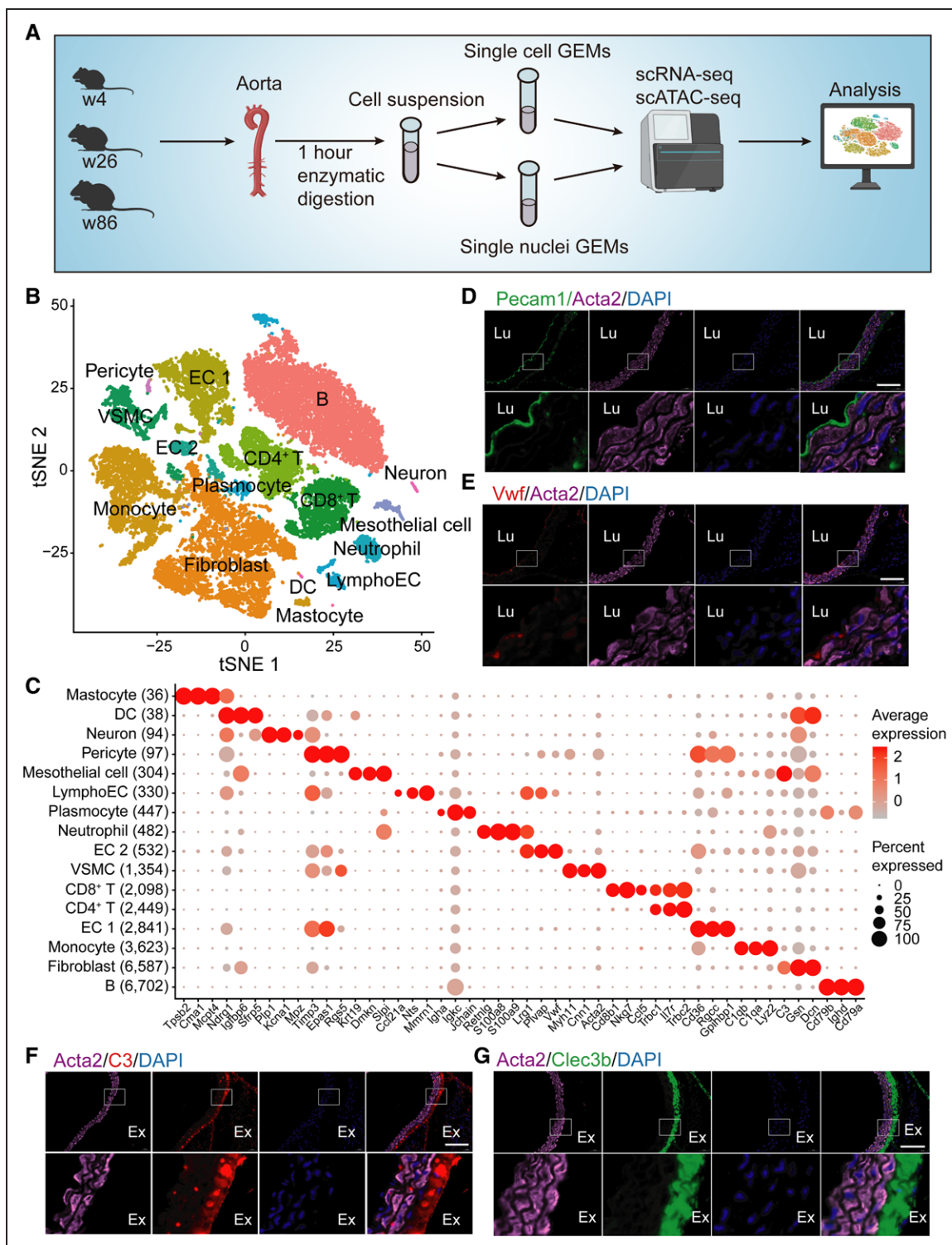
To identify cells with similar profiles, we applied 2000 variable genes per cell. Unsupervised graph clustering generated 16 cell groups, which were visualized using t-distributed stochastic neighbor embedding (Figure 2B). No major batch effect was observed as cells from each sample or different time points were relatively evenly distributed in clusters (Figure S1C and S1D). Each cluster was labeled for cell type with known marker genes. Vascular cell types represented in the distinct clusters included endothelial cell (EC) 1, EC 2, lymphoEC, vascular smooth muscle cells (VSMCs), fibroblasts, monocytes, plasmocytes, pericytes, mesothelial cells, and immune

cells such as dendritic cells, B cells, CD4 $^{+}$  T cells, CD8 $^{+}$  T cells, mastocytes, and neutrophils, as well as small neuronal clusters, likely arising from adjacent tissues.

Cell type-specific markers for each cluster were identified based on the genes with the highest differential expression relative to all other cells (Figure 2C). For example, the top 3 EC 1-specific markers were *Cd36*, *Rgcc*, and *Gpihbp1*, which are EC marker genes,<sup>11</sup> confirming the assignment of this cell cluster as EC 1. We also identified another EC cluster that highly expressed *Plvap* and *Vwf*, which we designated as the EC 2 cluster (Figure 2C). To determine whether EC 2 was an artifact of single-cell dissociation, an immediate-early gene set (including *Fos*, *Fobs*, *Jun*, *Junb*, and *Jund*) was evaluated. We found similar expression levels of immediate-early genes among EC 1 and EC 2 subtypes (Figure S2A), suggesting that EC 2 was a discrete subtype. Previously, Aditya et al<sup>12</sup> first reported the single-cell transcriptome atlas of normal mouse aorta and founded the 2 EC subtypes, CD36-expressing EC and VCAM1-expressing EC. Interestingly, by comparing EC markers, we observed that EC 1 had similar markers as those described for CD36-expressing EC, while EC 2 corresponded to the VCAM1-expressing EC (Figure S2B), further confirming the identities of EC 1 and EC 2. Meanwhile, *Vwf*, *Plvap*, and *Gpihbp1* represented the most specific and sensitive markers for distinguishing these 2 types of ECs (Figure 2C). However, the canonical EC marker *Pecam1* is sensitive for all ECs and, thus, cannot be used to distinguish different EC types (Figure S2C). As verified via immunofluorescence, all aortic ECs expressed *Pecam1* but not *Vwf*, which was previously described as a pan-EC marker (Figure 2D and 2E; Figure S2D). The expression analysis of *Pecam1* and *Vwf* in different EC subtypes based on another data set<sup>12</sup> further supported our findings (Figure S2B). Moreover, the previously described fibroblast marker *Serpinh1* was determined to not be specific (Figure S2C and S2E), whereas *C3* and *Clec3b* were specific for fibroblasts (Figure 2F and 2G; Figure S2F). Furthermore, *Acta2* and *Cnn1* were highly expressed only in VSMCs (Figure S2E and S2G).

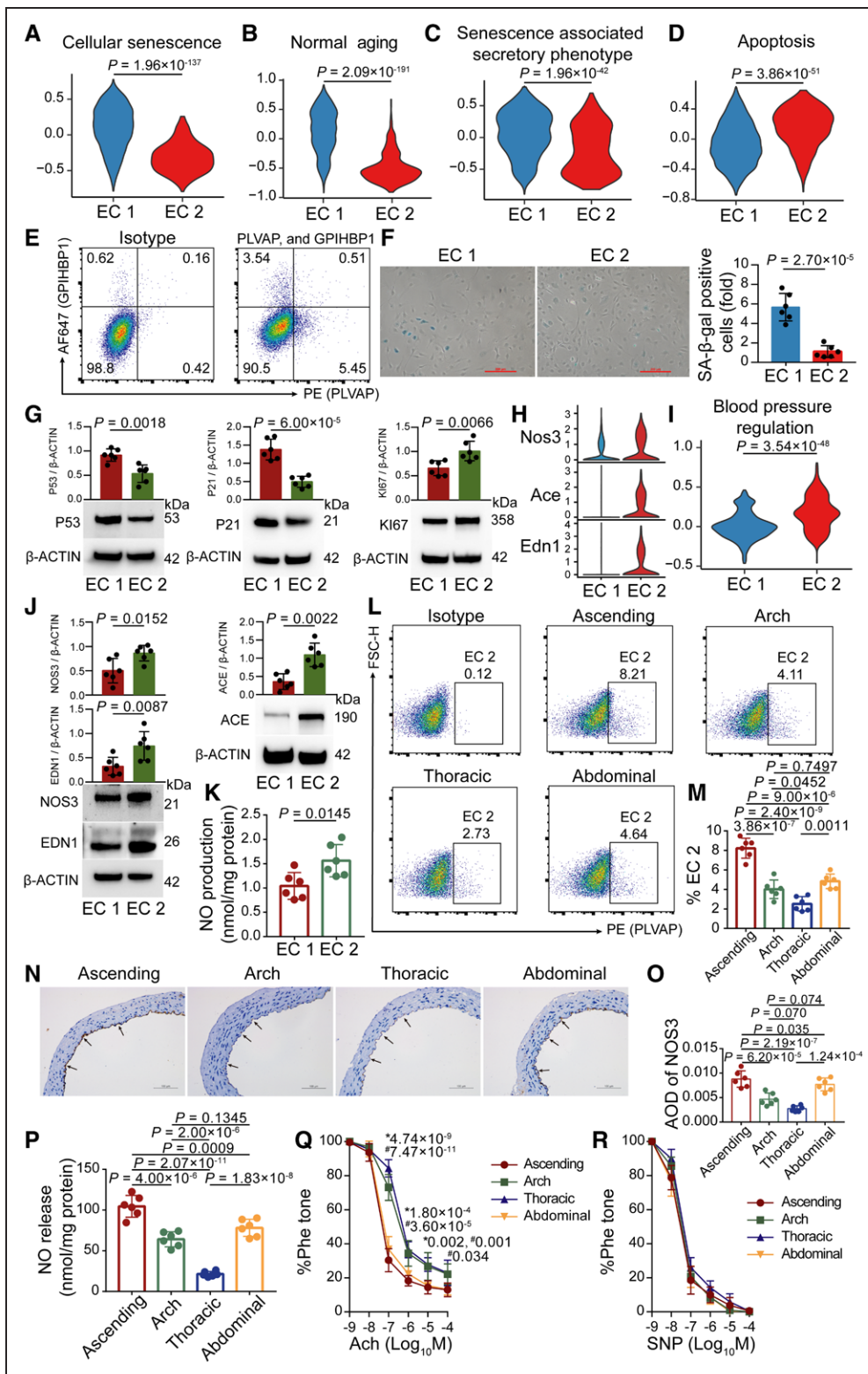
## Characteristics of Distinct EC Subtypes

Although gene ontology analysis<sup>13</sup> identified similar biological processes between the 2 types of vascular ECs (Figure S2H), gene set variation analysis<sup>14</sup> showed that they have different gene set activation scores. For example, EC 1 had a gene set more enriched in senescence and aging pathways compared with EC 2, whereas EC 2 exhibited higher apoptotic activity (Figure 3A through 3D). To verify this finding, GPIHBP1 $^{+}$  EC 1 and PLVAP $^{+}$  EC 2 were sorted and cultured based on fluorescence-activated cell sorting (Figure 3E). SA- $\beta$ -gal staining and Western blotting were subsequently performed revealing a higher percentage of SA- $\beta$ -gal positive cells and upregulation of the senescence-associated genes, *P53*



**Figure 2. Cell types identified using single-cell RNA sequencing (scRNA-seq) of aortic tissues in mice.**

**A**, Procedure flowchart. Two biological replicates for each time point (mice at 4, 26, and 86 wk of age) were used for single-cell experiments. **B**, Unsupervised graph clustering to partition the 28 014 cells into 16 clusters shown in a t-distributed stochastic neighbor embedding (t-SNE) diagram. n=6 mice. **C**, Dot plots of representative cell type-specific markers. Dot sizes represent the percentage of cells within a cluster expressing the gene; color represents gene expression level. The number on the left represents the cell number. n=6 mice. **D**, Representative immunofluorescence staining showing Pecam1 (marker for pan-endothelial cell [EC]) expression in endothelial cells from the thoracic aorta. n=6 mice. **E**, Representative immunofluorescence staining showing Vwf (marker for EC 2) expression in EC 2 from the thoracic aorta. n=6 mice. **F** and **G**, Representative immunofluorescence staining showing C3 and Clec3b (marker for fibroblasts) expression in fibroblasts from the thoracic aorta. Scale bars (**D–G**), 100  $\mu$ m. n=6 mice. B indicates B cell; DC, dendritic cell; Ex, extima; GEM, gel beads-in-emulsion; Lu, lumen; scATAC-seq, single-cell assay for transposase-accessible chromatin sequencing; and T, T cell.

**Figure 3. Distinct characteristics of endothelial cell (EC) subtypes.**

**A–D**, Gene set activity (associated with senescence, aging, and apoptosis pathways) of EC 1 (2841 cells from 6 mice) and EC 2 (532 cells from 6 mice) assessed using GSVA (gene set variation analysis). **E**, ECs were first collected based on aortic dissociation and magnetic-activated cell sorting (labeling with *Cd31* microbeads). CD31-positive ECs were then used for fluorescence-activated cell sorting (FACS). Six independent biological repeats (5 mice per repeat). **F**, SA-β-gal staining of EC 1 and EC 2. Six independent biological repeats. Scale bar, 200 μm. **G**, Western blotting of P53, P21, and KI67 protein levels in EC 1 and EC 2. Six independent biological repeats. **H**, Violin plot showing the expression of *Nos3*, *Ace*, and *Edn1* in EC 1 (2841 cells from 6 mice) and EC 2 (532 cells from 6 mice). **I**, Activity score of the blood pressure regulation pathway in EC 1 (2841 cells from 6 mice) and EC 2 (532 cells from 6 mice). **J**, Western blotting of *NOS3* (nitric oxide synthase 3), (Continued)

and *P21*, in EC 1 than EC 2, whereas downregulation of the proliferation-associated gene, *Ki67*, was observed in EC 1 compared with EC 2 (Figure 3F and 3G), suggesting that EC 1 plays a more crucial role in aortic aging than EC 2.

Functional analysis further demonstrated that EC 2 highly expressed genes involved in vascular tone regulation, such as *Nos3*, *Ace*, and *Edn1* (fold change: 1.510, 2.835, and 2.892, respectively, versus EC 1,  $P < 0.001$ ), and had increased gene set activity associated with blood pressure regulation compared with EC 1 (Figure 3H and 3I). These findings were also supported by results that EC 2 had increased abundance of NOS3 (nitric oxide synthase 3), ACE (angiotensin I-converting enzyme), and EDN1 (endothelin 1) and higher NO production in cell lysate than EC 1 (Figure 3J and 3K). To further explore the potential association between EC 2 and vascular tone regulation, the percentage of EC 2, NOS3 expression, NO content, and vasodilation function in different aortic anatomic locations (ascending, arch, thoracic, and abdominal) was assessed. Interestingly, a lower percentage of EC 2 and NOS3 expression was observed in the thoracic aorta compared with the other segments, whereas a higher percentage of EC 2 and NOS3 expression was observed in the ascending aorta (Figure 3L through 3O; Figure S2I). Additionally, the lower NO production and weaker Ach-induced (EC dependent) vasodilation were observed in the thoracic aorta compared with the ascending or abdominal segment (Figure 3P and 3Q). However, we did not observe differences in SNP-induced (EC independent) vasodilation among the 4 segments (Figure 3R). Collectively, these results indicated that different percentages of EC 2 across aortic segments might be associated with different EC-dependent vasodilation.

### Analysis of Cell Type-Specific Regulatory Networks Based on scRNA-Seq Data

To explore cell-specific gene regulatory networks and the activity associated with different TF (transcription factor) combinations, we used SCENIC (single-cell regulatory network inference and clustering)<sup>15</sup> and inferred the regulons (each representing a TF along with its coexpressed motif and significantly enriched target genes) and evaluated the activity score of regulons for each cell based on single-cell RNA-seq data. A total of 341 regulons were identified. Cell clustering based on the activity of these

regulons showed a lower cell resolution than Seurat t-distributed stochastic neighbor embedding projection; however, it separated the main cell types in the aortic tissue (Figure 4A). Specifically, cells in the different aortic layers, such as EC 1, VSMCs, and fibroblasts, had cell type-specific TF regulatory networks, while immune cells, including CD4<sup>+</sup> T and CD8<sup>+</sup> T cells, had shared regulatory states. For example, EC 1 had specific *Sox17* and *Klf3* regulatory networks, VSMCs had *Tead3* and *Srf* networks, and fibroblasts had *Tcf21* and *Msc* networks (Figure 4B). *Gata3* and *Snai3* were the common regulatory networks among CD4<sup>+</sup> T and CD8<sup>+</sup> T cells (Figure 4B). Moreover, we compared gene regulatory networks among all cell types in the aortic tissue (Figure S3) and observed that EC 1 and EC 2 had different regulatory circuitries (Figure S4A). Specifically, EC 2 had higher *Nr2f2*, *Lhx6*, *Dbp*, and *Nfia* regulon activity than EC 1, whereas EC 1 had higher *Klf7*, *Irx3*, *Pparg*, and *Gata2* regulon activity. Furthermore, the Kyoto Encyclopedia of Genes and Genomes pathway enrichment analysis<sup>13</sup> based on these TF target genes indicated that pathways involved in atherosclerosis, endocytosis, and autophagy were enriched in both EC 1 and EC 2 (Figure S4B). We also observed EC 1 to be significantly enriched in leukocyte trans-endothelial migration, platelet activation, and focal adhesion pathways and EC 2 to be primarily enriched in mitophagy, FoxO, longevity, and lipolysis-associated pathways, further indicating that EC 1 had a higher susceptibility to vascular inflammation during aging (Figure S4B).

### Aortic Aging Affects Cell Interaction, Inflammation, and Cell Type Composition

CellPhoneDB<sup>16</sup> analysis further revealed the cell-cell communication of aortic tissue changed with age. For example, a decrease in communication among VSMCs (distributed in the media layer of the aorta), fibroblasts (distributed in the adventitia layer of the aorta), and dendritic cells was observed in 86-week-old mice compared with 26-week-old mice; however, no significant changes were observed between 26- and 4-week-old mice (Figure S4C).

Given that EC dysfunction was a characteristic of VA, we further explored the communication network of EC 1 with other cell clusters and observed a decrease in communication between EC 1 and VSMCs, while that between EC 1 and monocytes increased with aortic aging (Figure 4C). These results corresponded with the Kyoto

**Figure 3 Continued.** ACE (angiotensin I-converting enzyme), and EDN1 (endothelin 1) protein levels in EC 1 and EC 2. Six independent biological repeats. **K**, NO level in cellular lysates of EC 1 and EC 2 detected using the Griess reagent. Six independent biological repeats. **L**, Representative flow cytometric analysis showing the percentage of EC 2 across 4 different aortic regions. **M**, Relative percentage of EC 2 across 4 different aortic regions. Six independent biological repeats (6 mice per repeat). **N** and **O**, The expression level of NOS3 across 4 aortic regions using IHC.  $n=6$  mice. **P**, NO level in tissues from 4 different aortic regions detected using the Griess reagent. Six independent biological repeats (5 mice at 26 wk of age per repeat). **Q**, Ach-induced endothelial-dependent relaxation in the 4 aortic regions.  $n=6$  mice. **R**, SNP-induced endothelial-independent relaxation in the aortic regions.  $n=6$  mice. \* $P$ , thoracic vs ascending; # $P$ , thoracic vs abdominal (**Q** and **R**). Data are expressed as mean  $\pm$  SD.  $P$  determined using the Mann-Whitney *U* test (**A–D** and **I**), 1-way ANOVA followed by the Bonferroni post test (**F**, **G**, **J**, **K**, **M**, **O**, and **P**), or 2-way repeated measures ANOVA followed by the Bonferroni post test (**Q** and **R**).

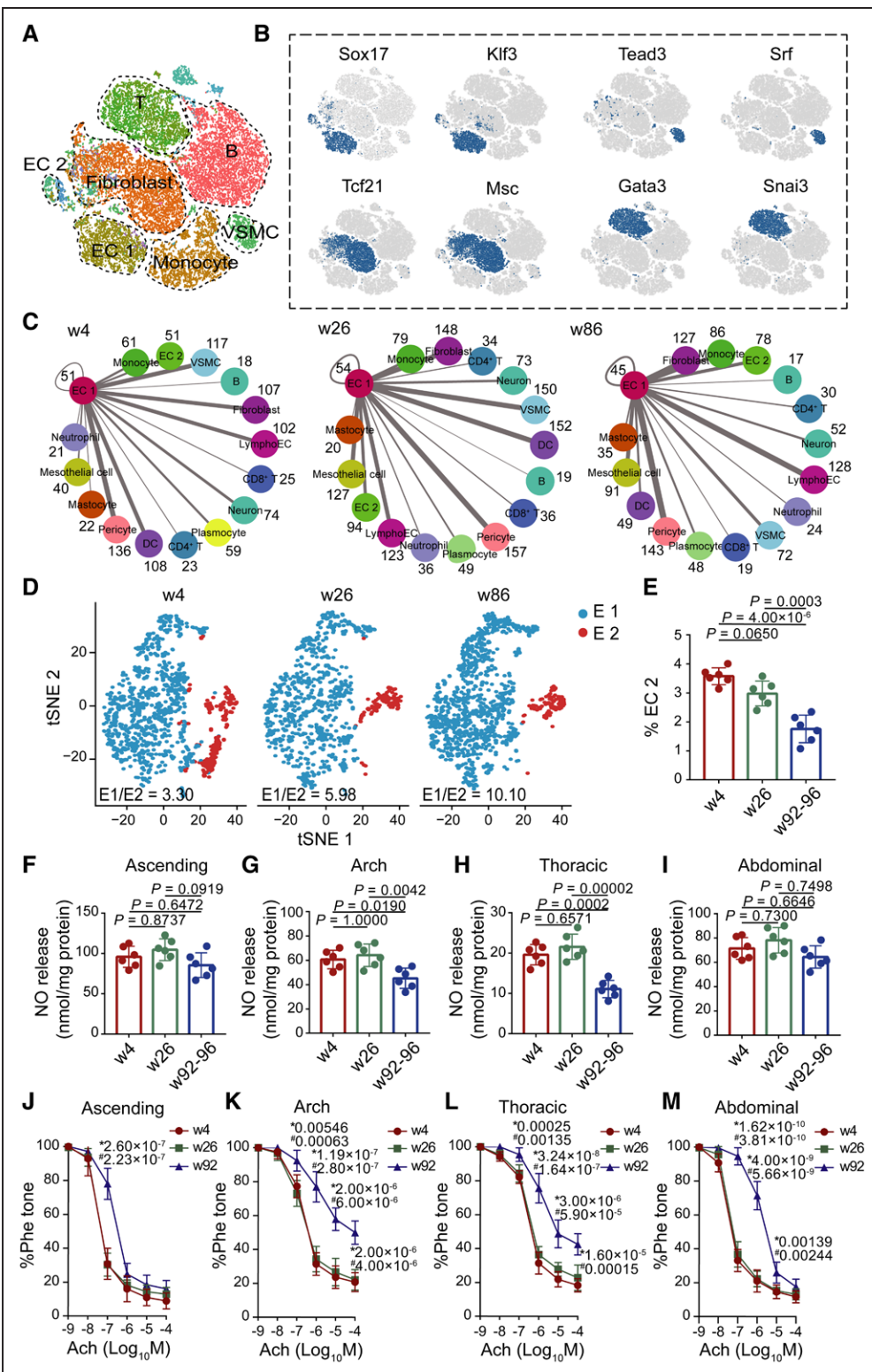


**Figure 4. Identification of cell type-specific gene regulatory networks using single-cell RNA sequencing (scRNA-seq).**

**A**, t-distributed stochastic neighbor embedding (t-SNE) projection for all sampled 28 014 cells based on regulon activity score (RAS). n=6 mice. **B**, Binarizes RAS (Z score normalization across all cells) for endothelial cell (EC) 1 (2841 cells from 6 mice)–specific regulons *Sox17* (cutoff value of 0.1 to convert to 0 and 1) and *Klf3* (cutoff value of 0.08) on t-SNE projection (blue-black dots); binarizes RAS for vascular smooth muscle cells (VSMCs; 1354 cells from 6 mice; cutoff value of 0.1 for *Tead3* and 0.11 for *Srf*); binarizes RAS for fibroblasts (6587 cells from 6 mice; cutoff value of 0.08 for *Tcf21* and 0.07 *Msc*); binarizes RAS for CD4<sup>+</sup> (2449 cells from 6 mice) and CD8<sup>+</sup> T cells (2098 cells from 6 mice; cutoff value of 0.03 for *Gata3* and 0.04 for *Snai3*). **C**, Connected line represents cell communication between EC 1 and other cell types. Line thickness is positively correlated with the number of ligand-receptor interaction events. (Continued)

Encyclopedia of Genes and Genomes pathway enrichment analysis results, indicating that ECs 1 were involved in leukocyte trans-endothelial migration. Interestingly, the EC 1:EC 2 ratio was elevated with increasing age, which was also supported by the fluorescence-activated cell sorting analysis of ECs from the thoracic aorta (Figure 4D and 4E; Figure S4D).

We then compared the NO content and EC-dependent and independent vasodilation among each age across different aortic segments. Results showed that arch and thoracic aorta from 92-week-old mice displayed lower NO production and weaker EC-dependent vasodilation compared with that from 4- and 26-week-old mice; however, no difference in the maximum relaxation to Ach was observed within ascending or abdominal aorta (Figure 4F through 4M). For EC-independent vasodilation, we did not observe differences across the 4 aortic segments (Figure S4E through S4H). Hence, the age-dependent imbalance in the EC 1:EC 2 ratio may influence vascular tone and blood pressure regulation. Moreover, TNF- $\alpha$  proinflammatory signaling was increased in EC 1, not in EC 2, in 86-week-old mice compared with 26-week-old mice (Figure S4I and S4J).

Considering that inflammation is a characteristic of tissue aging,<sup>17</sup> we further explored the dynamics of immune cells during aortic aging and observed that the percentage of neutrophils, plasmacytoid dendritic cells, and mastocytes increased with aortic aging, while the proportion of dendritic cells decreased in 86-week-old mice (Figure S5A). No significant change was observed in B cells, CD4 $^{+}$  T cells, CD8 $^{+}$  T cells, or monocytes (Figure S5A). In line with the immunohistochemistry results, levels of plasma inflammatory mediators, such as IL-1 $\beta$ , IL-6, and IL-10, were elevated in 86-week-old mice compared with 4- and 26-week-old mice (Figure S5B through S5D).

### Aortic Aging Reveals Increased Transcriptional Instability

Previous studies showed that aging results from increased transcriptional instability, while increased transcriptional noise is considered a characteristic of aging.<sup>18,19</sup> Thus, we quantified the transcriptional noise and senescence gene set<sup>20</sup> activity of the main cell types in the aortas of 4-, 26-, and 86-week-old mice. The earliest developmental stage that demonstrated an increase in transcriptional noise of EC 1, EC 2, and fibroblasts was

26 weeks. However, we did not observe an increase in the transcriptional noise of VSMCs (Figure 5A through 5D). Consistently, we observed that the senescence gene set activity of EC 1, EC 2, and fibroblasts exhibited an increase in senescence score with age, which was not observed for VSMCs (Figure 5E through 5H).

The resulting Venn diagram only identified 19 overlapping genes among the cell types with significantly different transcriptional stability observed between old and young mice, suggesting that genes related to high transcriptional variability were cell specific (Figure 5I). Pathway enrichment analysis of genes with increased transcriptional instability during aortic aging revealed that pathways related to cell cycle, gene transcription, and RNA polymerase II transcription were the most common features of the 3 cell types (Figure S5E). Furthermore, pathways related to transport of small molecules, endocytosis, and autophagy were significantly enriched in EC 1, whereas EC 2 showed enrichment of pathway terms related to metabolism, immune, and protein processing, suggesting that transcriptional instability might affect molecular transport, endocytosis, and autophagy functioning in EC 1 (Figure S5E).

### Weighted Gene Coexpression Network Analysis Identifies Aging-Related Gene Modules

To systematically investigate the transcriptional dynamics during aortic aging, we applied WGCNA (weighted gene coexpression network analysis)<sup>21</sup> to pseudocells (calculated from EC 1 and fibroblasts that have increased transcriptional noise during aortic aging and a sufficient number of cells, >2500).<sup>22</sup> For EC 1, a total of 2841 cells were converted to 280 pseudocells. Hierarchical cluster analysis showed that cells from the same age groups clustered well (Figure S6A). A coexpression network was then constructed, and 5 modules were identified, among which the turquoise module positively correlated with mouse age and had the largest correlation coefficient ( $r=0.81$ ,  $P=2\times 10^{-67}$ ; Figure S6B). Genes within the turquoise module were highly expressed in 86-week-old mice, and Kyoto Encyclopedia of Genes and Genomes analysis of the module genes suggested that atherosclerosis, leukocyte trans-endothelial migration, and certain inflammatory pathways were characteristic of EC 1 senescence (Figure 5J and 5K).

For fibroblasts, a total of 6587 cells were converted to 655 pseudocells. Similarly, hierarchical cluster analysis

**Figure 4 Continued.** Numbers indicate the events of ligand-receptor interaction for each intercellular link. Only those with a  $P$  cutoff of  $<0.05$  were considered to be real interactions. A total of 10 670 cells from 2 mice at 4 wk of age, 10 192 cells from 2 mice at 26 wk of age, and 7152 cells from 2 mice at 86 wk of age. **D**, t-SNE projection showing the EC 1:EC 2 ratio in mice at 4, 26, and 86 wk of age. A total of 1275 ECs from 2 mice at 4 wk of age, 875 ECs from 2 mice at 26 wk of age, and 1223 ECs from 2 mice at 86 wk of age. **E**, Relative percentage of EC 2 in mouse thoracic aorta for each time point detected by flow cytometric analysis. Six independent biological repeats (5 mice per repeat). **F–I**, NO levels across 4 different aortic regions detected using the Griess reagent. Six independent biological repeats (5 mice per repeat). **J–M**, Ach-induced endothelial-dependent relaxation in the ascending (**H**), arch (**I**), thoracic (**J**), and abdominal (**K**) aortic regions for each time point.  $n=6$  mice. \* $P$ , w92 vs w4; # $P$ , w92 vs w26 (**J–M**). Data are expressed as mean $\pm$ SD.  $P$  determined using 1-way ANOVA followed by the Bonferroni post hoc test (**E–I**) or 2-way repeated measures ANOVA followed by the Bonferroni post test (**J–M**).

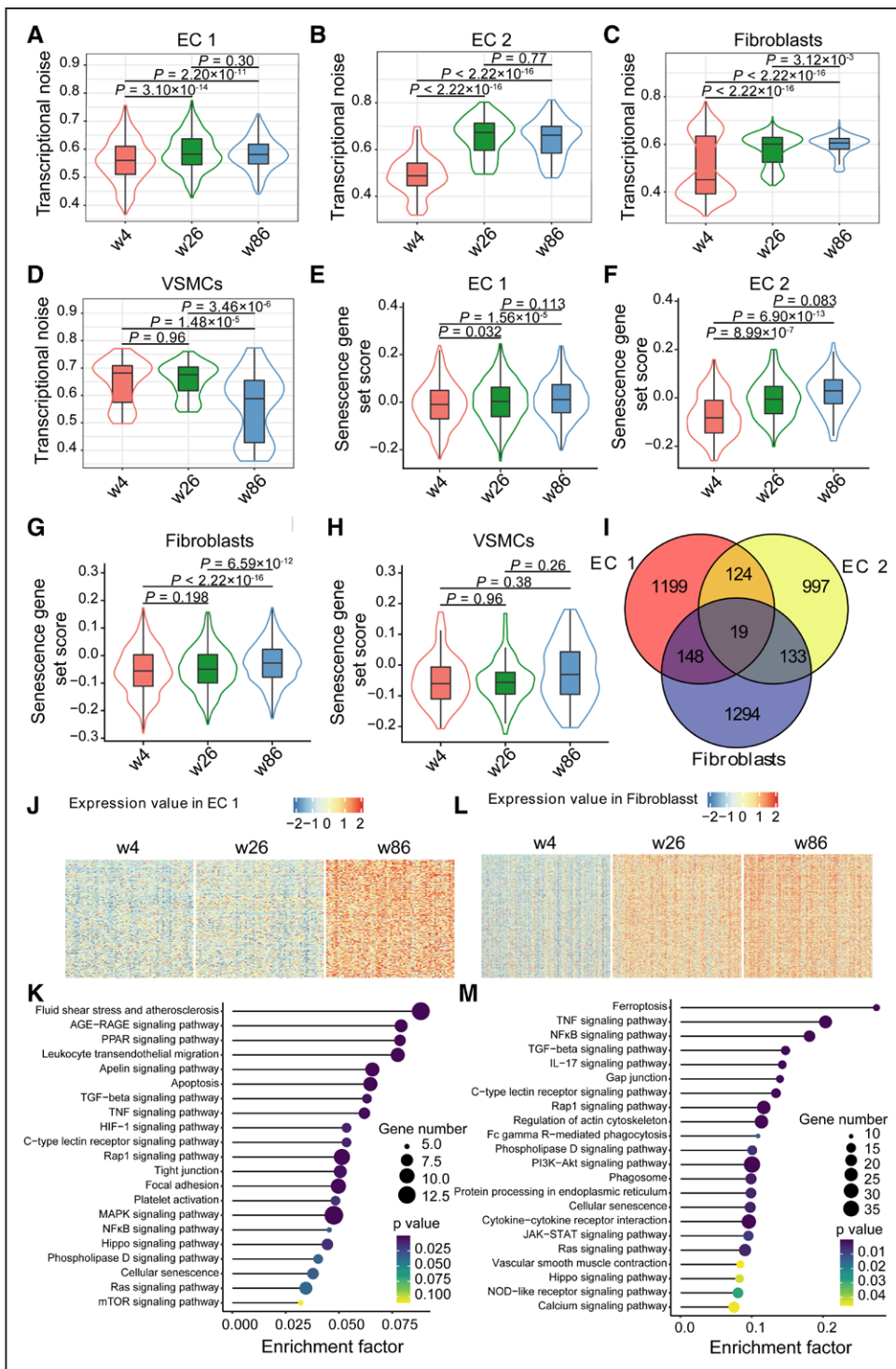


**Figure 5. Increased transcriptional noise and senescence-associated gene modules in aortic cells with aging.**

**A–D**, Violin plots illustrating transcriptional noise of endothelial cell (EC) 1 (750 cells per group), EC 2 (110 cells per group), fibroblasts (1375 cells per group), and vascular smooth muscle cells (VSMCs; 77 cells per group) from mice in different age groups. Cell numbers of each cell type in each age group were downsampled to equal cell numbers. **E–H**, Violin plot shows the senescence gene set activity score of EC 1 (750 cells per group), EC 2 (110 cells per group), fibroblasts (1375 cells per group), and VSMCs (77 cells per group) according to age. Cell numbers in each age group were downsampled to equal cell numbers. **I**, Venn diagram showing the overlapping genes with increased transcriptional instability among EC 1, EC 2, and fibroblasts. **J**, Heat map demonstrating the expression level of genes within the turquoise module in EC 1 (70 pseudocells per group, pseudocells numbers in each age group were downsampled to equal cell numbers) from mice with different age groups. **K**, The Kyoto Encyclopedia of Genes and Genomes (KEGG) pathway enrichment analysis based on genes within the turquoise module in EC 1. **L**, Heat map demonstrating the expression level of genes within the turquoise module in fibroblasts (100 pseudocells per group, pseudocell numbers in each age group were downsampled to equal cell numbers). **M**, KEGG pathway enrichment analysis based on genes within the turquoise module in fibroblasts. *P* was determined using the Kruskal-Wallis test followed by the Nemenyi post test (**A–H**).

showed that cells from the same groups clustered well (Figure S6C). WCGNA identified 2 modules. The turquoise module was positively correlated with mouse age ( $r=0.84$ ,  $P=8\times10^{-175}$ ; Figure S6D). Genes within the turquoise module were highly expressed in 26- and 86-week-old mice (Figure 5L). Moreover, the Kyoto Encyclopedia of Genes and Genomes analysis revealed that fibroblasts were enriched in many inflammatory pathways similar to EC 1, such as TNF- $\alpha$ , NF- $\kappa$ B (nuclear factor kappa B), and TGF- $\beta$  (transforming growth factor beta) pathways; however, the enriched pathways appeared at different ages (26 weeks; Figure 5M). Hence, fibroblasts might develop inflammatory senescence characteristics earlier than ECs.

### Single-Cell Chromatin Accessibility States of Aorta Tissue

Considering that bulk assay for transposase-accessible chromatin sequencing analysis only identifies accessibility regions of cis-regulatory elements at the population level, we performed 10 $\times$  scATAC-seq using aortic cells from the same samples to further explore cell type-specific regulatory signatures. Each sample was subjected to various stringent quality assessments and filtering (Figure S7A through S7C) to select high-quality nuclei. After performing quality control, we used Signac to integrate multiple samples and yield 142093 peaks associated with the chromatin accessibility region from 24329 cell nuclei (Table S2). Cells from each sample were relatively evenly distributed in all clusters, indicating no major batch effect (Figure S7D). To interpret the scATAC-seq data, we first created a gene activity matrix by assessing the chromatin accessibility associated with each gene body and 2 kb promoter region from the scATAC-seq data. We then used cross-modality integration and label transfer methods to calculate classification scores for each cell based on scRNA-seq data from the same biological sample. After filtering out nuclei with prediction scores  $<0.5$ , a total of 24188 nuclei remained for subsequent analysis. We observed that, apart from mastocytes, which had a small cluster and lower prediction score, all cell types from scATAC-seq data were well annotated (Figure 6A). The chromatin accessibility regions of all cell types were comprehensively characterized and located primarily in promoter, intron, and distal intergenic regions in all cell types, while differential cell types had differential feature proportions (Figure S7E). Chromatin accessibility signals were more abundant in the promoter region of immune cells compared with nonimmune cells, whereas nonimmune cells were more abundant in distal intergenic regions (Figure S7E). To obtain insights into the cell type-specific biological processes, differential accessibility peaks between cell clusters were identified. Cell type-specific TFs, identified based on scRNA-seq data, showed a higher DNA accessibility signal according to cell type, such as *Sox17* for EC 1, *Tead3* for VSMCs, and *Tcf21* for fibroblasts, suggesting that cell type maintenance

requires the coordinated action of cell type-specific TFs (Figure S7F through S7H). Similarly, for EC, we observed a higher DNA accessibility signal of *Sox17* in EC 1 and *Lhx6* in EC 2 (Figure S7I).

### Dynamics of Chromatin Accessibility During Aortic Aging

After revealing the aorta chromatin accessibility profiles, we compared the distribution of whole-genome chromatin accessibility signals in cells from mice of different ages. No noticeable changes were observed in the distribution of all peaks in EC 1 with age, with most peaks located in distal regions (10–100 kb) relative to the transcriptional start site (Figure 6B; Figure S8A). Similar results were observed in VSMCs and fibroblasts (Figure S8B through S8E). However, by comparing the levels of scATAC-seq peak signals in EC 1 among different age groups, differential accessibility regions, including increased accessibility regions (IARs) and decreased accessibility regions, were identified. For example, accessibility regions near *Tnf- $\alpha$* , *Il6*, *Arc*, and *Scd1* increased with age (Figure 6C through 6F). Both IARs and decreased accessibility regions in EC 1, VSMCs, or fibroblasts during aortic aging were proportionally more abundant in the promoter region ( $\leq 1$  kb relative to transcriptional start site) or distal intergenic region (Figure 6G and 6H; Figure S8F through S8I). Thus, aging might affect the degree of chromatin accessibility, particularly in the promoter and distal intergenic regions, more than the distribution of open chromatin regions.

To further understand the function of differential accessibility regions, we performed peak annotation and gene set enrichment analysis. Results showed that genes near IARs were primarily enriched in TNF- $\alpha$ /NF- $\kappa$ B, TGF- $\beta$ 1, and IL6/STAT3 (signal transducer and activator of transcription 3) signaling pathways (Figure 6I), which were activated during senescence.<sup>23</sup> Meanwhile, the genes near decreased accessibility regions are involved in metabolic processes and DNA repair (Figure 6I). Furthermore, to determine which TFs control the transcription of genes near IARs, motif enrichment analysis was performed and revealed *Atf3*, *Egr1*, and *Egr2* (Figure 6J) as regulators of senescence.<sup>8,24</sup> We also explored the dynamics of fibroblast chromatin accessibility, which had increased transcriptional noise during aortic aging. Gene set enrichment analysis of genes near IARs in fibroblasts showed enrichment in the TNFR1 pathway, whereas genes near decreased accessibility regions were enriched in cholesterol homeostasis, lysosome vesicle biogenesis, and cell-extracellular matrix interaction pathways (Figure S8J through S8N).

### Senescence Trajectory Analysis of Aorta ECs

To further explore the mechanism underlying EC 1 senescence, we extracted EC 1 from 6 samples, performed

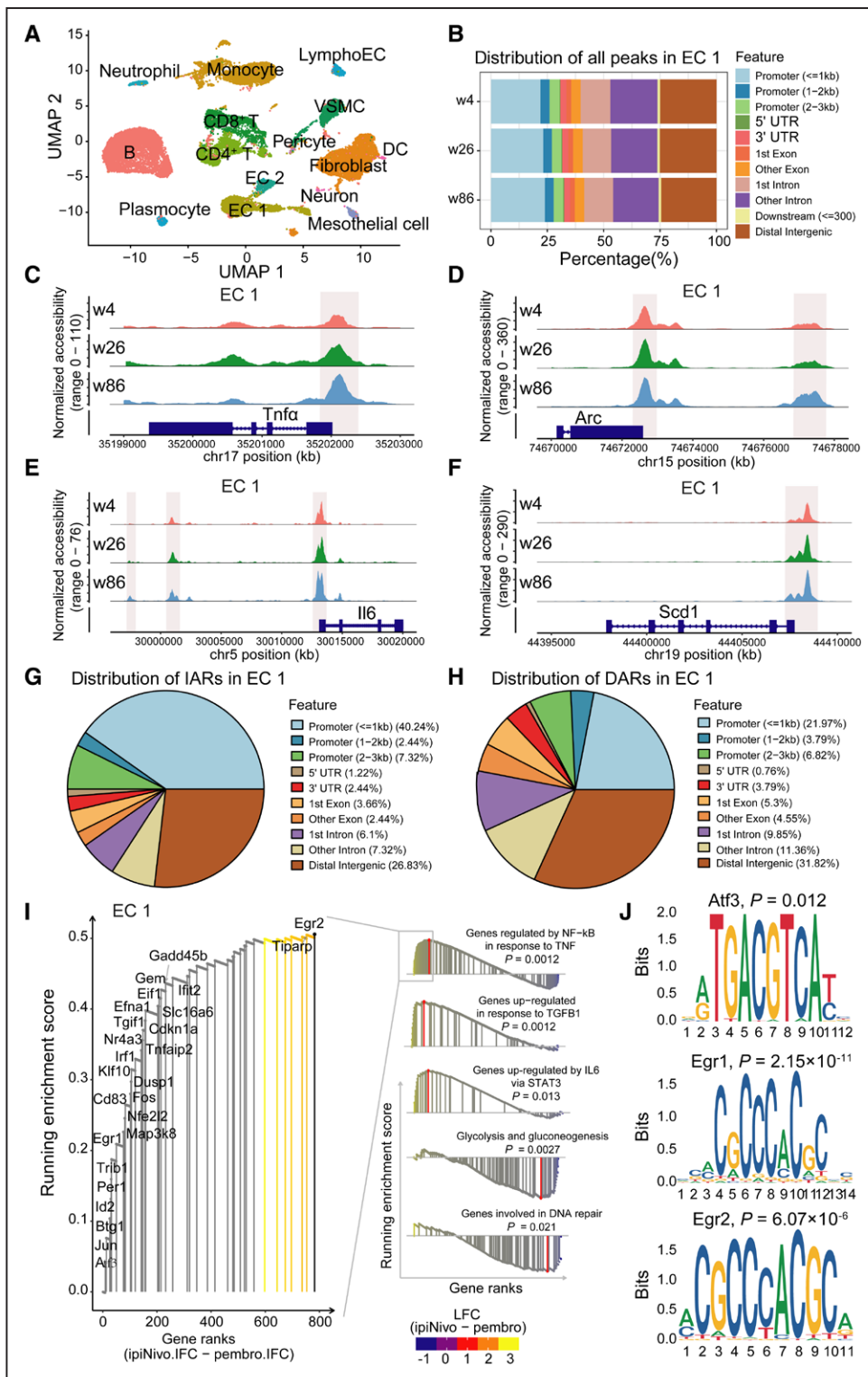


**Figure 6. Dynamics of chromatin accessibility during aortic aging.**

**A**, Uniform manifold approximation and projection (UMAP) visualization showing the distinct cell type clustering (a total of 24 188 nuclei from 6 mice) based on chromatin accessibility data. **B**, Genomic feature distributions of accessible chromatin regions in endothelial cell (EC) 1 among different age groups (499 nuclei for w4, 776 nuclei for w26, and 673 nuclei for w86). **C–F**, The genomic region of *Tnfa*, *Arc*, *Il6*, and *Scd1* showing ATAC-seq track of aggregate EC 1 (499 downsampled nuclei per group) from each age of mice. **G** and **H**, Genomic feature distributions of increased accessibility regions (IARs) and decreased accessibility regions (DARs) in EC 1 (499 nuclei for w4, 776 nuclei for w26, and 673 nuclei for w86). Bonferroni-adjusted  $P$  cutoff of 0.05. **I**, Rank-based gene set enrichment analysis of genes near differential accessibility regions in EC 1 (499 nuclei for w4, 776 nuclei for w26, and 673 nuclei for w86) during aortic aging. **J**, TF (transcription factor) motif enrichment analysis in IARs of EC 1. The height of the letters represented the frequency of each base in the cognate motif. LFC indicates log<sub>2</sub> fold change; and UTR, untranslated region.

stringent quality control, and merged multi-samples. The result of Uniform manifold approximation and projection showed that 2841 EC 1 from different age groups were evenly distributed, suggesting that merging multi-samples was effective (Figure S9A). Based on the reverse embedding graph algorithm,<sup>25</sup> Monocle2 recognized dynamic changes in gene expression patterns well and construction of pseudotime trajectory. Therefore, we applied Monocle2 to perform the pseudotime trajectory analysis in EC 1 and observed that pseudotime gradually increased from the prebranch of the trajectory to the end branch. Moreover, cells in the end branch primarily originated from older mice (86 weeks of age), suggesting that pseudotime of the trajectory reflected the gradual process of EC 1 senescence (Figure 7A and 7B). Next, to identify TFs potentially required to control corresponding cell states, we generated a list of 12 upregulated and 6 downregulated TFs correlated with the progression of pseudotime (Figure 7C).

It is of interest to determine whether the chromatin accessibility state of these TFs is consistent with the mRNA expression levels with the progression of pseudotime. Therefore, we performed pseudotime trajectory analysis based on the gene activity matrix with the same genes used in scRNA-seq data to order cells. The resultant heat map showed 18 motif accessibilities of indicated TFs during EC 1 senescence (Figure 7D). *Tead1*, *Gata2*, and *Mafk* exhibited consistent changes at the transcriptional and chromatin accessibility level, indicating that the increase in mRNA expression was related to the open chromatin in the promoter region. Additionally, mRNA expression of certain TFs did not match chromatin accessibility as exemplified for *Irf8* and *Eif4*, suggesting that other regulatory mechanisms might occur during EC 1 senescence (Figure 7C and 7D).

## Senescence Trajectory Analysis of Aorta Fibroblasts

We also explored the senescence mechanism of fibroblasts, as it is linked to heart aging.<sup>17</sup> Fibroblasts from all samples were extracted, and stringent QC was applied to remove low-quality cells. Uniform manifold approximation and projection results showed that 6691 fibroblasts from different age groups integrated well (Figure S9B). To further explore the dynamics of expression patterns in fibroblasts, pseudotime trajectory analysis was performed using Monocle2. With the advancing pseudotime, cells were separated into 2 branches, fate 1 and fate 2 (Figure 7E and 7F), which might be due to the transcriptional heterogeneity of fibroblasts during aging.<sup>17</sup> Gene ontology analysis of the highly expressed genes in cells from fate 1 showed enrichment in pathways involved in connective tissue development, muscle cell proliferation, and muscle adaptation, whereas the highly expressed genes in cells from fate 2 were primarily enriched in collagen metabolic and immunoinflammatory pathways (Figure 7G).

Next, to identify TFs potentially required to control corresponding cell fate, we identified 27 upregulated TFs correlated with advancing pseudotime in fate 1 (Figure 7H), as well as 16 upregulated and 5 downregulated TFs in fate 2 (Figure 7J). For example, the expression level of TFs, such as *Stat3*, *Nfil3*, and *Hoxa5*, increased with the advancing pesudotime, which might control the process of fibroblast senescence in fate 1.

To further explore the chromatin accessibility of these TFs, we aligned the TF motifs to pseudotime advancing (Figure 7I and 7K). Compared with EC 1, fibroblasts exhibited differently regulated TFs at the transcriptional and chromatin accessibility levels, indicating that cell type-specific TFs regulated aorta aging. Moreover, we observed that chromatin accessibility of most genes with increased transcriptional noise in EC 1 or fibroblasts had higher chromatin accessibility in the end stage of pseudotime advancing (Figure S9C and S9D).

## DISCUSSION

Inflamm-aging is the common pathological basis of age-related cardiovascular diseases<sup>26</sup>; thus, we investigated the altered proinflammatory state and cell senescence in the aorta with aging. Our data revealed that TNF- $\alpha$  gene set activity was increased in the EC 1 from aged mice, in line with previous findings indicating that tissue aging is accompanied by an increase in the inflammatory state.<sup>27–29</sup> Notably, we also found that EC 1 had a higher gene set activity in the senescence-associated secretory phenotype, whereas EC 2 had higher apoptosis (a noninflammatory mode of cell death) gene set activity, indicating that EC 1 had higher susceptibility to the inflamm-aging trait than EC 2. Although we described an increased ratio of EC 1 to EC 2, decreased NO production with aortic aging, and decreased EC-dependent vasodilation in aged mice, further investigations are required to explore the molecular mechanisms responsible for the imbalance between EC 1 and EC 2, as well as its subsequent influence on the function of EC-dependent vasodilation.

Previous studies have demonstrated that aging is accompanied by increased transcriptional noise, including within the human pancreas,<sup>18</sup> mouse immune cells,<sup>19</sup> mouse heart,<sup>17</sup> and primate arteries.<sup>30</sup> In this study, we observed increased transcriptional noise of EC 1 in the aortic intima layer and fibroblasts in the aortic adventitia layer, consistent with the findings of Zhang et al.<sup>30</sup> However, we did not observe increased transcriptional noise or senescence gene set activity in the VSMCs of aged mice, indicating that VSMCs might be less sensitive to senescence-induced damage or that their elimination was more effective than that of EC 1 and fibroblasts in the aorta. Moreover, the higher chromatin accessibility signals of most genes with increased transcriptional noise were observed in end stage pseudotime advancing, indicating that transcriptional noise might result

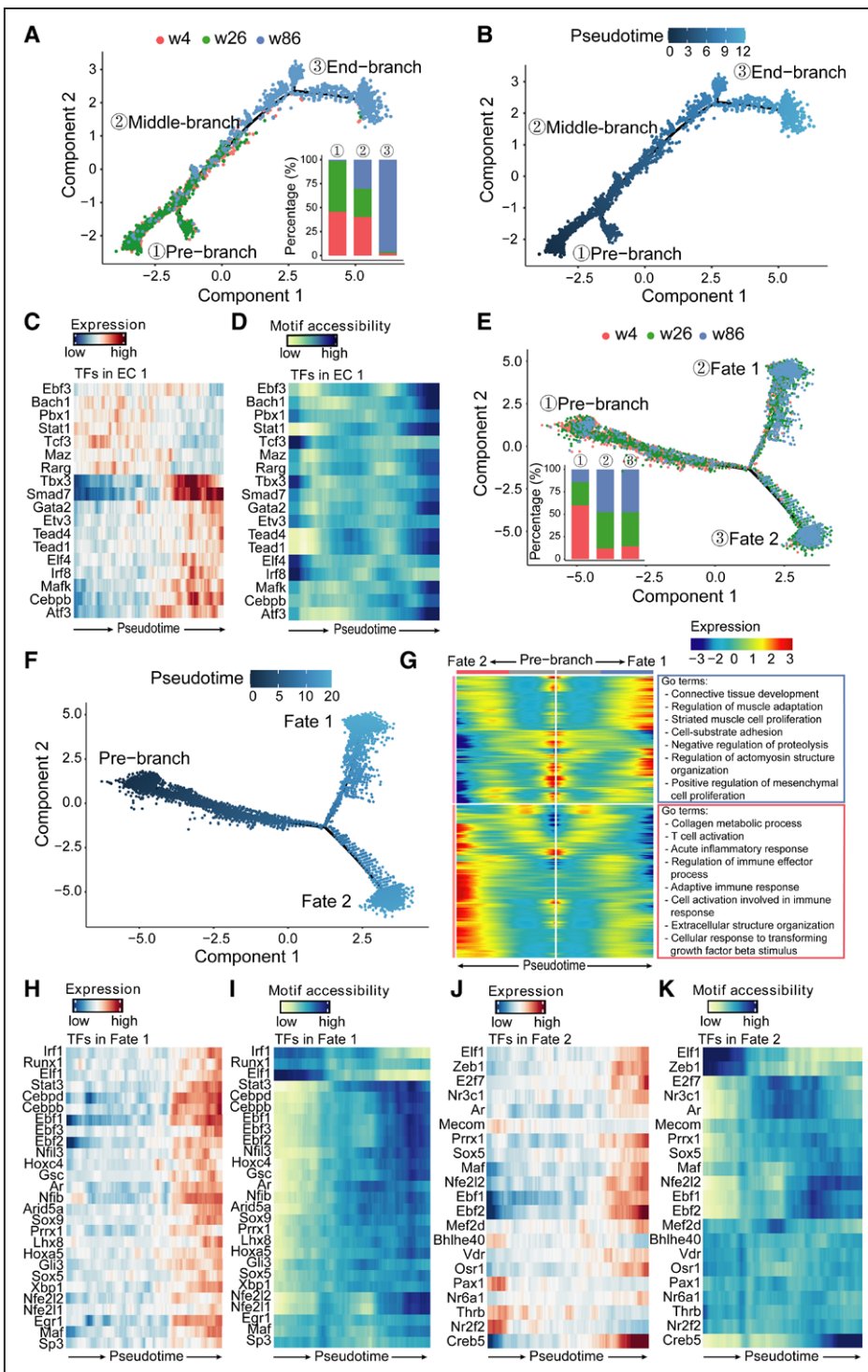


**Figure 7. Senescence trajectory analysis of endothelial cell (EC) 1 and fibroblasts.**

**A**, EC 1 (2841 cells from 6 mice) on the pseudotime tree is color-coded by age. Histogram showing the relative proportions of EC 1 from 4-, 26-, and 86-wk-old mice on each branch in the pseudotime tree. **B**, EC 1 (2841 cells from 6 mice) on the pseudotime tree is color-coded by pseudotime. Genes within the turquoise module associated with the senescence of EC 1 were used to construct the pseudotime tree. **C**, Smoothed heat map demonstrating the dynamic changes of RNA expression of indicated TFs (transcription factors) during EC 1 (2841 cells from 6 mice) senescence. **D**, Smoothed heat map demonstrating the dynamic changes of motif accessibility of indicated TFs during EC 1 (1948 nuclei from 6 mice) senescence. **E**, Fibroblasts (6587 cells from 6 mice) on the pseudotime tree are color-coded by age. **F**, Fibroblasts (6587 cells from 6 mice) on the pseudotime tree are color-coded by pseudotime. The genes within the turquoise module associated with fibroblast senescence were selected to construct the pseudotime tree. **G**, Heat map of the relative expression of differentially expressed genes between fate 1 and fate 2 cells (**left**) and corresponding representative gene ontology terms ( $P$  adjusted,  $<0.05$ ) of fate 1 and fate 2 cells (**right**). A total of 6587 fibroblasts from 6 mice. **H** and **I**, Same as **C** and **D** but for fate 1 branch in fibroblasts from 6 mice. **J** and **K**, Same as **C** and **D** but for fate 2 branch in fibroblasts from 6 mice.

from an imbalance in epigenetic regulation. Hence, further in-depth investigations are required to decipher the molecular mechanisms associated with the increased transcriptional noise observed during aortic aging.

The imbalance of epigenetic mechanisms has been linked to aging syndrome in model organisms.<sup>31</sup> Unlike DNA mutations, epigenetic changes are, theoretically, reversible. Therefore, identifying cell type-specific, or conservative, changes in chromatin accessibility states during aging is of great significance. Although chromatin remodeling has been linked to cardiovascular aging and atherosclerosis, dynamic alterations in the genome-wide chromatin accessibility atlas at the single-cell level have not been systematically characterized for aortic aging.<sup>32</sup> Based on our scATAC-seq data, we found that each cell population possessed differential chromatin accessibility states, suggesting that chromatin accessibility profiles represent powerful tools to distinguish cellular heterogeneity. Moreover, we identified numerous matching RNA:ATAC (assay for transposase-accessible chromatin) TF pairs in EC 1 and fibroblasts, which likely function to regulate cellular senescence. For example, *Atf3* was found to drive EC senescence by reconstructing accessible chromatin profiles,<sup>8</sup> verifying our results. Moreover, among the upregulated TFs in fibroblasts, *Stat3* is involved in neuroinflammation by upregulating *Bace1* expression.<sup>33</sup> Meanwhile, *Stat3* inhibition reduces the expression of proinflammatory mediators, including IL-6, IL1 $\beta$ , and TNF- $\alpha$ , in the brain.<sup>33</sup> These results suggest that these upregulated proinflammatory TFs may participate in aortic inflamm-aging.

Certain limitations were noted in this study. First, using an enzyme cocktail to digest tissue likely induced artifactual transcriptional stress responses, while certain cell types might be vulnerable to digestion, thereby increasing cell loss<sup>34</sup>; as such, the aortic wall would have been digested for only 1 hour to reduce the enzyme-dissociated associated bias. Moreover, the aorta media was more difficult to digest than the intima and adventitia, causing a lower proportion of VSMCs than expected. Therefore, our data might not represent the actual proportion of cells in the aorta, particularly regarding VSMCs. There are 2 potential solutions for the enzyme-dissociated associated bias, namely, application of cold-dissociation or single-nucleus RNA sequencing for hard-to-dissociate aortic samples.<sup>35,36</sup> Second, the perivascular adipose tissue was preserved when harvesting the mouse aorta; however, we did not observe lipocytes. This might be due to the floating characteristic of lipocytes in liquid and loss during the preparation of aortic dissociation. The relatively high number of immune cells in the aorta may primarily arise from the perivascular adipose tissue, which contains a variety of immune cells.<sup>37</sup> Third, all samples in this study were obtained from male mice, and a relatively small sample size was used. Thus, studies with large sample sizes are required to further

explore sex-independent differences. Taken together, the integration of single-cell RNA-seq and assay for transposase-accessible chromatin sequencing data provided a comprehensive understanding of aortic aging at the single-cell level.

## ARTICLE INFORMATION

Received March 31, 2021; accepted November 23, 2021.

### Affiliation

Department of Geriatrics, Department of Cardiac Surgery, and Department of Cardiology, Fujian Heart Disease Center, Fujian Medical University Union Hospital, Fuzhou, China (W.X., Q.Y., J.L., L.C., J.F., X.C., Y.Z., L.C., H.H.). Fujian Key Laboratory of Vascular Aging, Fujian Medical University, Fuzhou, China (W.X., Y.K., D.L., H.H.). Fujian Institute of Geriatrics, Fujian Medical University Union Hospital, Fuzhou, China (W.X., Y.K., D.L., H.H.).

### Sources of Funding

This work was financially supported by the National Natural Science Foundation of China (81570448, 81800422, and 82071560), the Joint Funds of Scientific and Technological Innovation Program of Fujian Province (2017Y9055 and 2019Y9086), National Key Clinical Specialty Discipline Construction Programs (2013544), and Fujian Province's Key Clinical Specialty Discipline Construction Programs (2012149).

### Disclosures

None.

### Supplemental Material

Supplemental Methods

Figures S1–S9

Tables S1–S2

Major Resources Table

References 38–49

## REFERENCES

- Dantas AP, Jiménez-Altayó F, Vila E. Vascular aging: facts and factors. *Front Physiol*. 2012;3:325. doi: 10.3389/fphys.2012.00325
- Donato AJ, Machin DR, Lesniewski LA. Mechanisms of dysfunction in the aging vasculature and role in age-related disease. *Circ Res*. 2018;123:825–848. doi: 10.1161/CIRCRESAHA.118.312563
- Wu C, Zheng L, Wang Q, Hu Y. The emerging role of cell senescence in atherosclerosis. *Clin Chem Lab Med*. 2020;59:27–38. doi: 10.1515/cclm-2020-0601
- Chen LW, Dai XF, Lu L, Zhang GC, Cao H. Extensive primary repair of the thoracic aorta in acute type a aortic dissection by means of ascending aorta replacement combined with open placement of triple-branched stent graft: early results. *Circulation*. 2010;122:1373–1378. doi: 10.1161/CIRCULATIONAHA.110.946012
- Chen LW, Wu XJ, Lu L, Zhang GC, Yang GF, Yang ZW, Dong Y, Cao H, Chen Q. Total arch repair for acute type A aortic dissection with 2 modified techniques: open single-branched stent graft placement and reinforcement of the dissected arch vessel stump with stent graft. *Circulation*. 2011;123:2536–2541. doi: 10.1161/CIRCULATIONAHA.110.008656
- Cochain C, Vafadarnejad E, Arampatzis P, Pelisek J, Winkels H, Ley K, Wolf D, Saliba AE, Zernecke A. Single-cell RNA-seq reveals the transcriptional landscape and heterogeneity of aortic macrophages in murine atherosclerosis. *Circ Res*. 2018;122:1661–1674. doi: 10.1161/CIRCRESAHA.117.312509
- He D, Mao A, Zheng CB, Kan H, Zhang K, Zhang Z, Feng L, Ma X. Aortic heterogeneity across segments and under high fat/salt/glucose conditions at the single-cell level. *Natl Sci Rev*. 2020;7:881–896. doi: 10.1093/nsr/nwaa038
- Zhang C, Zhang X, Huang L, Guan Y, Huang X, Tian XL, Zhang L, Tao W. ATF3 drives senescence by reconstructing accessible chromatin profiles. *Aging Cell*. 2021;20:e13315. doi: 10.1111/acel.13315
- Stuart T, Butler A, Hoffman P, Hafemeister C, Papalexi E, Mauck WM 3rd, Hao Y, Stoeckius M, Smibert P, Satija R. Comprehensive integration of single-cell data. *Cell*. 2019;177:1888–1902.e21. doi: 10.1016/j.cell.2019.05.031

10. Barron M, Li J. Identifying and removing the cell-cycle effect from single-cell RNA-Sequencing data. *Sci Rep.* 2016;6:33892. doi: 10.1038/srep33892
11. Kalucka J, de Rooij LPMH, Goveia J, Rohlenova K, Dumas SJ, Meta E, Conchinha NV, Taverna F, Teuwen LA, Veys K, et al. Single-cell transcriptome atlas of murine endothelial cells. *Cell.* 2020;180:764–779.e20. doi: 10.1016/j.cell.2020.01.015
12. Kalluri AS, Vellarikkal SK, Edelman ER, Nguyen L, Subramanian A, Ellinor PT, Regev A, Kathiresan S, Gupta RM. Single-cell analysis of the normal mouse aorta reveals functionally distinct endothelial cell populations. *Circulation.* 2019;140:147–163. doi: 10.1161/CIRCULATIONAHA.118.038362
13. Yu G, Wang LG, Han Y, He QY. clusterProfiler: an R package for comparing biological themes among gene clusters. *OMICS.* 2012;16:284–287. doi: 10.1089/omi.2011.0118
14. Hänzelmann S, Castelo R, Guinney J. GSVA: gene set variation analysis for microarray and RNA-seq data. *BMC Bioinformatics.* 2013;14:7. doi: 10.1186/1471-2105-14-7
15. Aibar S, González-Blas CB, Moerman T, Huynh-Thu VA, Imrichova H, Hulselmans G, Rambow F, Marine JC, Geurts P, Aerts J, et al. SCENIC: single-cell regulatory network inference and clustering. *Nat Methods.* 2017;14:1083–1086. doi: 10.1038/nmeth.4463
16. Efremova M, Vento-Tormo M, Teichmann SA, Vento-Tormo R. CellPhoneDB: inferring cell-cell communication from combined expression of multi-subunit ligand-receptor complexes. *Nat Protoc.* 2020;15:1484–1506. doi: 10.1038/s41596-020-0292-x
17. Vidal R, Wagner JUG, Braeuning C, Fischer C, Patrick R, Tombor L, Muhly-Reinholz M, John D, Kliem M, Conrad T, et al. Transcriptional heterogeneity of fibroblasts is a hallmark of the aging heart. *JCI Insight.* 2019;4:e131092. doi: 10.1172/jci.insight.131092
18. Enge M, Arda HE, Mignardi B, Beausang J, Bottino R, Kim SK, Quake SR. Single-cell analysis of human pancreas reveals transcriptional signatures of aging and somatic mutation patterns. *Cell.* 2017;171:321–330.e14. doi: 10.1016/j.cell.2017.09.004
19. Martinez-Jimenez CP, Eling N, Chen HC, Vallejos CA, Kolodziejczyk AA, Connor F, Stojic L, Rayner TF, Stubbington MJT, Teichmann SA, et al. Aging increases cell-to-cell transcriptional variability upon immune stimulation. *Science.* 2017;355:1433–1436. doi: 10.1126/science.aah4115
20. Zhao M, Chen L, Qu H. CSGene: a literature-based database for cell senescence genes and its application to identify critical cell aging pathways and associated diseases. *Cell Death Dis.* 2016;7:e2053. doi: 10.1038/cddis.2015.414
21. Langfelder P, Horvath S. WGCNA: an R package for weighted correlation network analysis. *BMC Bioinformatics.* 2008;9:559. doi: 10.1186/1471-2105-9-559
22. Tosches MA, Yamawaki TM, Naumann RK, Jacobi AA, Tushev G, Laurent G. Evolution of pallium, hippocampus, and cortical cell types revealed by single-cell transcriptomics in reptiles. *Science.* 2018;360:881–888. doi: 10.1126/science.aar4237
23. Hernandez-Segura A, Nehme J, Demaria M. Hallmarks of cellular senescence. *Trends Cell Biol.* 2018;28:436–453. doi: 10.1016/j.tcb.2018.02.001
24. Tyler EJ, Gutierrez Del Arroyo A, Hughes BK, Wallis R, Garbe JC, Stampfer MR, Koh J, Lowe R, Philpott MP, Bishop CL. Early growth response 2 (EGR2) is a novel regulator of the senescence programme. *Aging Cell.* 2021;20:e13318. doi: 10.1111/ace.13318
25. Trapnell C, Cacchiarelli D, Grimsby J, Pokharel P, Li S, Morse M, Lennon NJ, Livak KJ, Mikkelsen TS, Rinn JL. The dynamics and regulators of cell fate decisions are revealed by pseudotemporal ordering of single cells. *Nat Biotechnol.* 2014;32:381–386. doi: 10.1038/nbt.2859
26. Fougère B, Boulanger E, Nourhashémi F, Guyonnet S, Cesari M. Chronic inflammation: accelerator of biological aging. *J Gerontol A Biol Sci Med Sci.* 2017;72:1218–1225. doi: 10.1093/gerona/glw240
27. Ma S, Sun S, Geng L, Song M, Wang W, Ye Y, Ji Q, Zou Z, Wang S, He X, et al. Caloric restriction reprograms the single-cell transcriptional landscape of *rattus norvegicus* aging. *Cell.* 2020;180:984–1001.e22. doi: 10.1016/j.cell.2020.02.008
28. Consortium TM. A single-cell transcriptomic atlas characterizes aging tissues in the mouse. *Nature.* 2020;583:590–595. doi: 10.1038/s41586-020-2496-1
29. Schaum N, Lehallier B, Hahn O, Pállovics R, Hosseinzadeh S, Lee SE, Sit R, Lee DP, Losada PM, Zardeneta ME, et al; Tabula Muris Consortium. Ageing hallmarks exhibit organ-specific temporal signatures. *Nature.* 2020;583:596–602. doi: 10.1038/s41586-020-2499-y
30. Zhang W, Zhang S, Yan P, Ren J, Song M, Li J, Lei J, Pan H, Wang S, Ma X, et al. A single-cell transcriptomic landscape of primate arterial aging. *Nat Commun.* 2020;11:2202. doi: 10.1038/s41467-020-15997-0
31. Zhang W, Qu J, Liu GH, Belmonte JCI. The ageing epigenome and its rejuvenation. *Nat Rev Mol Cell Biol.* 2020;21:137–150. doi: 10.1038/s41580-019-0204-5
32. Zhang W, Song M, Qu J, Liu GH. Epigenetic modifications in cardiovascular aging and diseases. *Circ Res.* 2018;123:773–786. doi: 10.1161/CIRCRESAHA.118.312497
33. Millot P, San C, Bennana E, Porte B, Vignal N, Hugon J, Paquet C, Hosten B, Mouton-Liger F. STAT3 inhibition protects against neuroinflammation and BACE1 upregulation induced by systemic inflammation. *Immunol Lett.* 2020;228:129–134. doi: 10.1016/j.imlet.2020.10.004
34. van den Brink SC, Sage F, Vértesy Á, Spanjaard B, Peterson-Maduro J, Baron CS, Robin C, van Oudenaarden A. Single-cell sequencing reveals dissociation-induced gene expression in tissue subpopulations. *Nat Methods.* 2017;14:935–936. doi: 10.1038/nmeth.4437
35. Grindberg RV, Yee-Greenbaum JL, McConnell MJ, Novotny M, O'Shaughnessy AL, Lambert GM, Araúzo-Bravo MJ, Lee J, Fishman M, Robbins GE, et al. RNA-sequencing from single nuclei. *Proc Natl Acad Sci USA.* 2013;110:19802–19807. doi: 10.1073/pnas.1319700110
36. Adam M, Potter AS, Potter SS. Psychrophilic proteases dramatically reduce single-cell RNA-seq artifacts: a molecular atlas of kidney development. *Development.* 2017;144:3625–3632. doi: 10.1242/dev.151142
37. Kumar RK, Jin Y, Watts SW, Rockwell CE. Naïve, regulatory, activated, and memory immune cells co-exist in PVATs that are comparable in density to non-PVAT fats in health. *Front Physiol.* 2020;11:58. doi: 10.3389/fphys.2020.000058
38. Ke Y, Li D, Zhao M, Liu C, Liu J, Zeng A, Shi X, Cheng S, Pan B, Zheng L, et al. Gut flora-dependent metabolite trimethylamine-N-oxide accelerates endothelial cell senescence and vascular aging through oxidative stress. *Free Radic Biol Med.* 2018;116:88–100. doi: 10.1016/j.freeradbiomed.2018.01.007
39. Li D, Ke Y, Zhan R, Liu C, Zhao M, Zeng A, Shi X, Ji L, Cheng S, Pan B, et al. Trimethylamine-N-oxide promotes brain aging and cognitive impairment in mice. *Aging Cell.* 2018;17:e12768. doi: 10.1111/acel.12768
40. Xie WH, Ding J, Xie XX, Yang XH, Wu XF, Chen ZX, Guo QL, Gao WY, Wang XZ, Li D. Hepatitis B virus X protein promotes liver cell pyroptosis under oxidative stress through NLRP3 inflammasome activation. *Inflamm Res.* 2020;69:683–696. doi: 10.1007/s00011-020-01351-z
41. Zou Z, Long X, Zhao Q, Zheng Y, Song M, Ma S, Jing Y, Wang S, He Y, Esteban CR, et al. A single-cell transcriptomic atlas of human skin aging. *Dev Cell.* 2021;56:383–397.e8. doi: 10.1016/j.devcel.2020.11.002
42. Tirosh I, Izar B, Prakadan SM, Wadsworth MH 2nd, Treacy D, Trombetta JJ, Rotem A, Rodman C, Lian C, Murphy G, et al. Dissecting the multicellular ecosystem of metastatic melanoma by single-cell RNA-seq. *Science.* 2016;352:189–196. doi: 10.1126/science.aad0501
43. Yu G, Wang LG, He QY. ChIPseeker: an R/Bioconductor package for ChIP peak annotation, comparison and visualization. *Bioinformatics.* 2015;31:2382–2383. doi: 10.1093/bioinformatics/btv145
44. Fang H, De Wolf H, Knezevic B, Burnham KL, Osgood J, Sanniti A, Lledó Lara A, Kasela S, De Cesco S, Wegner JK, et al; ULTRA-DD Consortium. A genetics-led approach defines the drug target landscape of 30 immune-related traits. *Nat Genet.* 2019;51:1082–1091. doi: 10.1038/s41588-019-0456-1
45. Liberzon A, Subramanian A, Pinchback R, Thorvaldsdóttir H, Tamayo P, Mesirov JP. Molecular signatures database (MSigDB) 3.0. *Bioinformatics.* 2011;27:1739–1740. doi: 10.1093/bioinformatics/btr260
46. Han X, Zhou Z, Fei L, Sun H, Wang R, Chen Y, Chen H, Wang J, Tang H, Ge W, et al. Construction of a human cell landscape at single-cell level. *Nature.* 2020;581:303–309. doi: 10.1038/s41586-020-2157-4
47. Jia G, Preussner J, Chen X, Guenther S, Yuan X, Yekelchyk M, Kuenne C, Looso M, Zhou Y, Teichmann S, et al. Single cell RNA-seq and ATAC-seq analysis of cardiac progenitor cell transition states and lineage settlement. *Nat Commun.* 2018;9:4877. doi: 10.1038/s41467-018-07307-6
48. Verfaillie A, Imrichova H, Janký R, Aerts S. iRegulon and i-cisTarget: reconstructing regulatory networks using motif and track enrichment. *Curr Protoc Bioinformatics.* 2015;52:2.16.1–2.16.39. doi: 10.1002/0471250953.bi0216s52
49. Suo S, Zhu Q, Saadatpour A, Fei L, Guo G, Yuan GC. Revealing the critical regulators of cell identity in the mouse cell atlas. *Cell Rep.* 2018;25:1436–1445.e3. doi: 10.1016/j.celrep.2018.10.045